ACS APPLIED MATERIALS & INTERFACES

Research Article

www.acsami.org

Morphological Changes of Tungsten Surfaces by Low-Flux Helium Plasma Treatment and Helium Incorporation via Magnetron Sputtering

Santhosh Iyyakkunnel,[†] Laurent Marot,*[,†] Baran Eren,[†] Roland Steiner,[†] Lucas Moser,[†] Daniel Mathys,[‡] Marcel Düggelin,[‡] Patrick Chapon,[§] and Ernst Meyer[†]

[†]Department of Physics, University of Basel, Klingbergstrasse 82, 4056 Basel, Switzerland

[‡]Centre of Microscopy, University of Basel, Klingelbergstrasse 50/70, 4056 Basel, Switzerland

[§]Horiba Jobin Yvon, 16-18, rue du Canal, 91165 Longjumeau, France

ABSTRACT: The effect of helium on the tungsten microstructure was investigated first by exposure to a radio frequency driven helium plasma with fluxes of the order of 1 × 10^{19} m^{-2} s^{-1} and second by helium incorporation via magnetron sputtering. Roughening of the surface and the creation of pinholes were observed when exposing poly- and nanocrystalline tungsten samples to low-flux plasma. A coating process using an excess of helium besides argon in the process gas mixture leads to a porous thin film and a granular surface structure whereas gas mixture ratios of up to 50% He/Ar (in terms of their partial pressures) lead to a dense structure. The presence of helium in the deposited film was confirmed with glow-discharge optical emission spectroscopy and thermal desorption measurements. Latter revealed that the highest fraction of the embedded helium atoms desorb at approximately 1500 K. Identical plasma treatments at various temperatures showed strongest modifications of the surface at 1500 K, which is attributed to the massive activation of helium singly bond to a single vacancy inside the film. Thus, an efficient way of preparing nanostructured tungsten surfaces and porous tungsten films at low fluxes was found.

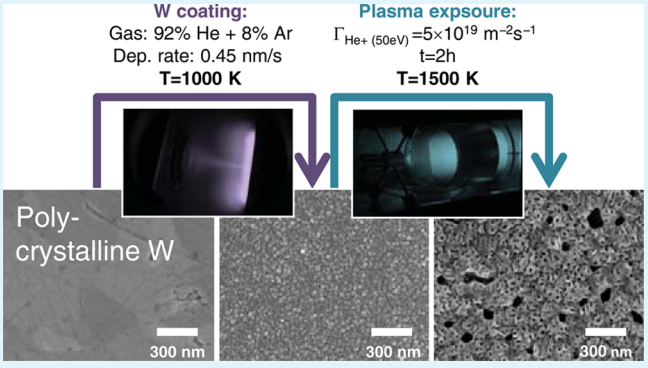

KEYWORDS: *nanostructuring, surface modification, helium plasma, tungsten, magnetron sputtering*

INTRODUCTION

Surface nanostructuring has attracted a great deal of interest in the last decades, because of its exceptional material properties. These newly obtained mechanical, optical, and electronic properties mainly stem from the nanometer-sized microstructures (grains, filaments, etc.) and the enhanced number of interfaces.[1,2] The resultant higher surface area to volume ratio is especially desirable in fields like energy conversion and storage, catalysis and sensing.[3] For instance, nanostructured materials achieve higher rates of the electrode reaction in lithium-ion batteries,[4] and have a higher efficiency in the photoelectrochemical splitting of water.[5,6] It was already reported that tungsten surfaces were nanostructured by low-energy helium ions for solar water splitting applications.[7] Especially for catalytic purposes, three-dimensional porosity is preferable to an array of tubes which has a one-dimensional character.[8] Moreover, a high degree of nanostructuring of metal surfaces (black metals) can also result in ideal light absorption rendering it highly beneficial in solar-thermal applications such as thermophotovoltaic systems, where the conversion of sunlight to heat is used.[9,10] However, for latter application, withstanding large heat loads is a prerequisite, which tungsten can easily meet because of its high melting point.[10]

A very efficient way of tungsten nanostructuring was discovered in the fusion community as a consequence of its bombardment with energetic helium atoms (or ions), which will be a byproduct of the fusion reaction between deuterium and tritium in the next generation fusion reactors (e.g., ITER and DEMO). In ITER for example, tungsten is planned to be used for the divertor plate and dome structures, thanks to the low sputtering yield, the low tritium retention and the high melting point.[11]

The tendril formation on tungsten first reported by Takamura et al.,[12] so-called "fuzz" tungsten, can be detrimental for the fusion reactors. However, it offers us an elegant solution for fabricating highly nanostructured and porous surfaces for the above-mentioned applications. A "fuzz" structure by modification of tungsten surfaces by what is assumed to be a consequence of formation and growth of helium bubbles can exhibit the highest surface area to volume ratio without extra effort. This renders nanostructuring using this method of great potential. Formation of "fuzz"-like structures are not limited to

Received: April 18, 2014
Accepted: June 24, 2014
Published: June 24, 2014

tungsten as similar structures upon helium bombardment were also observed on other metals such as molybdenum, nickel, titanium, stainless steel, and iron.[8,13] In general, microstructural changes on metals induced by high-energy (in the range of keV) ion bombardment have long been reported using typical linear implanter.[14,15] However, in contrast to exposure to plasma, this technique is directional and time-consuming. The challenge to be tackled is yet to achieve an efficient way of nanostructuring in laboratory setups, in which only milder conditions are accessible compared to those in linear plasma devices or fusion reactors.

The experiments performed so far in literature with linear plasma devices (PISCES,[16−19] NAGDIS[11,20] or Pilot-PSI[21]) can shed light on a recipe for laboratory helium plasma exposure experiments. First of all, this filament structure was only observed after bombarding tungsten surfaces at elevated temperatures (1000 K $\leq T \leq$ 2000 K) with He ions.[16,21,22] Second, the ion energy was chosen to be lower than the sputtering threshold in order not to induce any damage via sputtering. It was also reported that a threshold energy of about 20 eV has to be surmounted in order for nanostructuring to take place.[22] Depending on the flux, this threshold may increase to around 37 eV.[19] Finally, strong indications of a certain required flux (in the order of 1×10^{21} m^{-2} s^{-1}) for an effective fuzz formation were reported.[17,23] This is the typically limited parameter in ordinary laboratory setups, which is the main reason nanostructuring in such systems is a real challenge.

In this work, the effect of helium implantation in polycrystalline tungsten and thin tungsten films is investigated and thereby, a promising bottom-up approach of tungsten nanostructuring with a common laboratory helium plasma is presented. The implantation is achieved via low-flux He plasma treatment ($\sim 1 \times 10^{19}$ m^{-2} s^{-1}) and/or deposition of tungsten films in a helium-rich environment. Although, both processes were efficient methods to load tungsten with helium leading to porous and highly corrugated morphologies, the strongest nanostructuring was obtained when the surface temperature of a helium-loaded tungsten thin film was set to 1500 K during plasma treatment. This temperature corresponds to He occupying a single vacancy, at which also the most intense peak was observed in our thermal desorption measurements. The results presented in this work offer a reproducible way of controlling surface corrugation of tungsten at the nanoscale, which also exhibits many similarities to an early stage of fuzz growth.

EXPERIMENTAL SECTION

Polycrystalline tungsten (Pc W) disks from Plansee with a diameter of 30 mm and a thickness of 1 mm were both used as substrates for coatings and as samples to be exposed to plasma. The disks were polished using abrasive SiC paper, diamond paste and finally alumina oxide with a particle size of 0.05 μm resulting a typical roughness R_a of ∼1.4 nm. Afterward, the substrates were ultrasonically cleaned with acetone and ethanol before being introduced to high vacuum. Both, the coatings and the plasma exposures, were performed at the plasma facilities at the University of Basel.[24] A conventional pumping system was used to reach a background pressure of 5×10^{-5} Pa, which was also supported by liquid nitrogen trapping for selective trapping of residual gas (oxygen, carbon, etc.). The sample surface could be heated up to 1000 K with a resistive boron nitride heater attached to the backside of the sample holder.

The nanocrystalline (Nc) coatings were prepared on aforementioned Pc W disks by means of pulsed-DC (50 kHz, 496 ns) magnetron sputtering operated at 150 W (if not stated otherwise) using either argon, helium or a mixture of both as process gas. The target was a 3.5 in. wide W disk with a purity of 99.9%. The working pressure was set to 1.1, 4.1, and 1.87 Pa for Ar, He and the mixture, respectively. In the case of mixtures, the percentage of He was calculated from the ratio of the partial pressures of the involved gases. In the following, only the percentage of He will be stated. The target−sample distance was ∼5 cm in order to increase the deposition rate, especially when pure He was used. The deposition rate was estimated using a quartz microbalance (QMB) and the duration of the deposition was adjusted for a film thickness of 250 nm.

A radio frequency (RF, 13.56 MHz) plasma was discharged in an asymmetric capacitively coupled configuration placing the sample on the powered electrode. To cope with the instabilities of this plasma, a second plasma source (surfatron)[25] was mounted to the vacuum vessel and was operated at 150 W. The ion fluxes of plasmas in the chamber, obtained from Langmuir probe measurements at a distance of around 5 cm away from the sample surface, were $\sim 4.8-5.3 \times 10^{19}$ m^{-2} s^{-1}. The plasma had a typical ion density of $\sim 1.2 \times 10^{16}$ m^{-3} and electron temperatures of 7−8 eV. The plasma treatment experiments were performed continuously for 7200 s.

A new custom-built high vacuum system was used for experiments at temperatures exceeding 1000 K. The substrates were (3 or 6) × 30 × (0.1 or 0.2) mm^3 W stripes, trough which direct currents were driven to reach surface temperatures as high as 2500 K. Nanocrystalline coatings, in this case, were prepared in the first experimental setup and were transferred after breaking the vacuum to the new system. The samples were treated with plasma generated with the external plasma source (surfatron) while a negative bias was applied on them to set the acceleration potential of the He$^+$ ions. This high-T facility also allowed us to perform time and temperature controlled thermal desorption measurements. For this configuration, a Pfeiffer SmartTest leak tester was connected to the turbomolecular pump of the chamber. The temperature and the He leak-rate were recorded simultaneously. The temperature measurement was performed through viewports of the vacuum vessel using a pyrometer (MAURER IR-AHIS/600−3000 °C) using an emissivity of 0.1. Measurements of the specular reflectivity using a using a Varian Cary 5 spectrophotometer in the wavelength range of 250−2500 nm revealed a decrease of only few percent after plasma exposure. As explained by Kirchhoffs law,[26] the emissivity is 1 minus the specular reflectivity leading to only a minor change of the emissivity in our case. Moreover, the temperature was controlled on witness sample with a spot-welded thermo−element of the surface.

Plasma parameters such as He$^+$ ion flux and the plasma potential measured at the plasma facility are not expected to vary greatly in the custom-built high-T facility as similar plasma sources were used.

The surface morphology of the films were examined with a Hitachi S-4800 scanning electron microscope (SEM), whereas the cross-sections in panels c and f in Figure 1 were taken with a NanoLab 600 Helios (FEI company) device, which is a combined SEM and focused ion beam (FIB) facility using 30 keV Ga$^+$ ions for cutting. A layer of 500 nm platinum (Pt) was used to protect the sample surface at the cross-section edge. The samples were further investigated with glow-discharge optical emission spectroscopy (GDOES) using a GD Profiler 2 (Horiba Jobin Yvon) with neon (Ne) as plasma gas and operating conditions leading to an erosion rate of around 6.5 μm/min. X-rays diffractograms (XRD) were recorded using a SIEMENS D500 instrument with monochromatic Cu Kα radiation (40 kV and 30 mA) at a glancing incidence of 5°. With this setup, the calculated thickness of a W film through which only 10% of the incident light intensity will be transmitted is 606 nm, i.e., the measured signal is mostly coming from the deposited film.

RESULTS AND DISCUSSION

Compact Structures Exposed to a Low-Flux Helium Plasma. Polycrystalline and nanocrystalline W were exposed to an RF driven helium plasma. RF was applied directly onto the sample generating a self-bias of −50 V, lending He ions an average impact energy of roughly 100 eV (plasma potential V_p

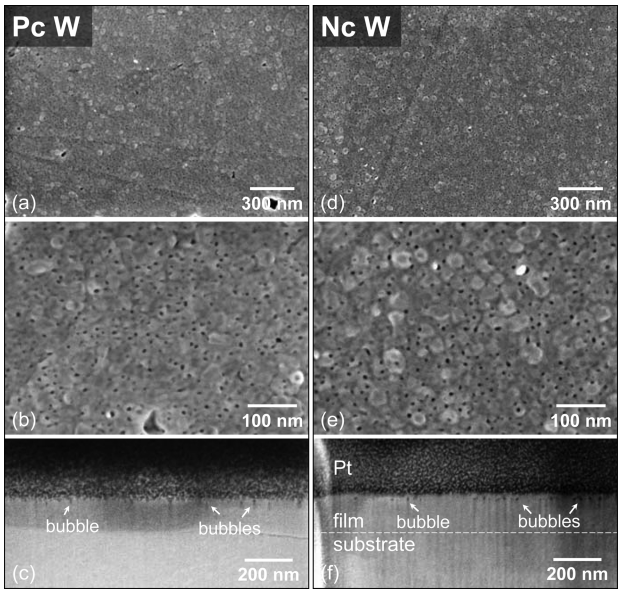

Figure 1. Top view SEM images of (a, b) a Pc W substrate and (d, e) a Nc W coating (RT, 0.58 nm/s) exposed to an RF-driven He plasma with a self-bias of −50 V for 2 h. (c, f) Cross-sections performed by FIB. A protective platinum (Pt) layer was deposited locally onto the surface.

≅ 50 V). The samples were exposed to plasma for 7200 s, during which the sample was heated to around 1000 K.

Figure 1 shows the results of the plasma treatment on Pc W on the left panel, and Nc W on the right panel. The Nc W film was deposited on a Pc W substrate at room temperature (RT) using a pure Ar gas process which led to growth of a compact structure. The outcomes after the plasma treatment were very similar to each other as pinholes of similar sizes (few nm) were observed on both samples. Furthermore, the rather flat surfaces of Nc and Pc W got roughened after the plasma treatment with He. In case of Pc W, the roughness R_a, as measured with atomic force microscopy, increased from 1.4 nm before the plasma treatment to 2.9 nm after the treatment. A similar change was observed for Nc W. With diameters around 7−10 nm, the pinholes are also slightly bigger on Nc W than on Pc W, on which an average pinhole size of about 5−6 nm was found. The obtained features on the surface can be attributed to He bubble formation beneath the surface due to implantation of He as a result of the ion bombardment.

In Figure 1c, f, cross-sections of the samples created by FIB are presented. Presence of bubbles just below the surface can be observed. The bubbles are located at a depth of 15−20 nm beneath the surface, which is an indication of bulk diffusion of He, because the mean implantation depth of He in W for 100 eV ions is only about 1.7 nm according to SRIM calculations.[27] Even though many pinholes are also observed on the Pc W sample, only few bubbles can be seen in the cross-section (Figure 1f). Additionally, with a size of up to 13 nm, bubbles observed in the Nc W are much bigger than those observed in Pc W (7 nm).

Because of the low solubility of He in W, the interstitial diffusion of He atoms in W lattice is very fast, even at RT.[28] If not trapped inside the material, mobile He atoms will escape through near external surfaces. Grain boundaries, defects or impurities, thereby, act as good trapping sites in the material.[18,29] The potential well formed by such a trap is able to bind multiple He atoms, which promotes the nucleation of He clusters and bubbles. The high pressure built up by the growing bubble induces a transformation of the trap by moving adjacent W atoms from their initial lattice site in order to release the stress. The newly formed mobile interstitial W atoms migrate to near external surfaces giving rise to the observed roughening. Origin of the pinholes is believed to result from bubbles close to the surface rupturing a thin layer of W above them.[30] The increased structuring on Nc W can probably be attributed to the higher density of traps, such as grain boundaries, offering a larger storage capacity for He. A higher fraction of entrapped He is also assumed to have caused the apparently larger pinholes on the top view images (Figure 1a−d) and bubbles in the cross sections (Figure 1e, f). This is in accordance with the study of Baldwin et al.,[18] which investigates the effect of (high-flux) He plasma ($\Gamma_{He^+} \cong 5 \times 10^{22}$ m^{-2} s^{-1}) on various W grades and claims highest rates of nanostructure formation on samples where trap concentrations, such as defects or grain boundaries, are high. The fact that fuzz-like structures were also observed on single-crystalline W, which should virtually have no defects, suggests a self-driven trapping mechanism where displacements of W atoms from their lattice positions are caused by accumulation of He and growth of He bubbles. It is assumed that defects are necessary for efficient nanostructuring. They can also be induced by irradiation or thermal damage.[18,31] In summary, even though the flux of the He plasma used in the current work is a factor of 100 or 1000 smaller than what is generally used to grow the fuzz structure, surface modifications and pinholes as a result of He bubble formation can already be observed. The surface structuring can be assumed to be the early stage in the fuzz growth process.

Helium Loading during Coating. Another way of loading W with He is including it directly during the thin film growth process. In this part, the effect of the He content in the process gas on the film morphology during the coating process is investigated. Top view SEM images of the results are presented in Figure 2a−d along with XRD patterns for the corresponding coatings. The XRD pattern of a reference polished Pc W substrate annealed at 1000 K is also given.

Figure 2a shows an image of a W coating prepared without He, on which different sized grains ranging from few 100 nm to few μm are visible. For this sample, it should be noted that the deposition rate was 1.78 nm/s (higher than other coatings) as a consequence of the higher sputtering yield of Ar on W than that of He.[32] The thickness was ca. 250 nm for all samples expect the sample in Figure 2d as the use of pure He diminished the deposition rate greatly. Judging from the XRD patterns (top panel), one can argue the existence of an epitaxial relationship between the Pc W substrate and the deposited film without He, which is not seen when He is added in the process. It should be stated that the average information depth measured by XRD, the so-called $1/e$ is 275 nm with conditions we used. Visually, a similar structure as in Figure 2a was observed for 50% He (Figure 2b), even though the XRD measurements revealed the intensity distribution be more alike of a polycrystalline film without any preferential orientation.[33] For this coating, a lower power of the magnetron was used (50 W) to obtain a comparable deposition rate (0.68 nm/s) with the next coating (Figure 2c). The small crystals observable on the first two coating might be precipitation of crystals of W compounds formed with impurities such as oxygen or carbon.

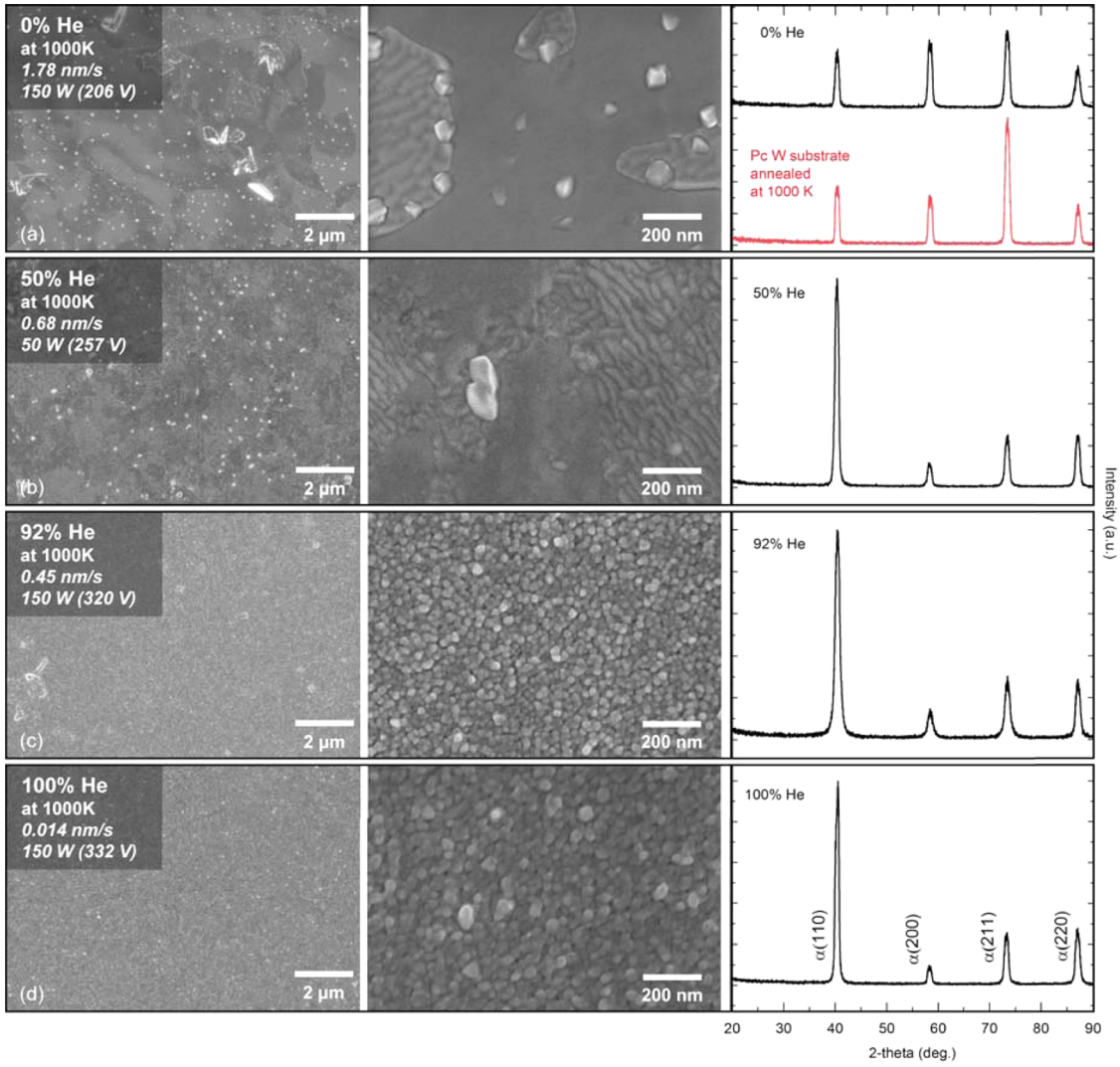

Figure 2. Top-view SEM images of W coatings deposited with (a) 0, (b) 50, (c) 92, and (d) 100% He. All coatings were prepared at a surface temperature of 1000 K. The deposition rate as well as the magnetron power and the discharge voltage are given in the corresponding image. XRD patterns are given for the coatings and for a Pc W substrate annealed at 1000 K for 2 h for comparison.

The morphology changes drastically when the helium content in the process gas mixture is about 92% (Figure 2c) compared to 0% or 50% He films resulting in compact structures. The small amount of argon here is necessary for igniting and maintaining the plasma for magnetron sputtering. The coating had a fine granular morphology with the features having dimensions of few tens of nanometers. Like in the other works,[34,35] igniting the magnetron with pure He was not possible. Deposition with pure He could, however, be achieved when another plasma was generated with an external source aiding the ignition of the magnetron. Once the magnetron started running, the external plasma was turned off. Deposition with pure He results in a surface morphology very similar to that with 92% He; however, the deposition rate suffered from the lack of Ar which has a higher sputtering yield on W for a given ion energy.[32] The deposition rate in this case was reduced from 0.45 nm/s to about 0.014 nm/s. For the two latter samples, XRD patterns also resemble the intensity distribution of Pc W without a preferential orientation.

Figure 3 shows cross-sectional SEM images of a W coating prepared with 92% He on a silicon substrate at 1000 K. The silicon substrate is usually covered with native oxide of about 3 nm thickness. With this image, the effect of having a high percentage of He in the process gas, like in the top-view SEM images c and d in in Figure 2, is illustrated more strongly. A thoroughly porous film when using 92% He is achieved in contrast to the dense structure of a nanocrystalline W film that is obtained by using pure Ar at the very elevated temperature.[36] Dense, mostly columnar structures is typical for a metallic coating using Ar as process gas, which is formed due limited grain boundary mobility at the base of the film.[36,37] Even

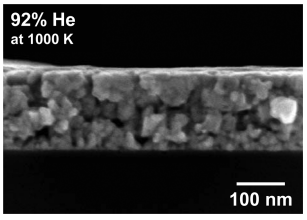

Figure 3. Cross-section SEM image of Nc W film deposited on silicon using 92% He in the process gas mixture. The surface temperature was set to 1000 K, whereas the deposition rate was 0.56 nm/s at a magnetron power of 150 W.

though one can argue that the energy of W neutrals also affect the morphology of the film, it is believed that the growth process of the porous structure obtained is strongly affected by the high amount of He present in the process gas and therefore is different from the conventional growth process.

The ability to incorporate helium much more efficiently than argon into growing films with sputter deposition techniques such as magnetron sputtering is mainly due to the difference of energy the atom possesses after being backscattered from the target. During magnetron sputtering, the target is eroded by accelerated ions bombarding the surface inducing ejection of target atoms (sputtering) via a collision cascade. A fraction of the gas atoms arriving at the target is however neutralized and backscattered into the vacuum chamber.[35] Assuming an ideal elastic collision of gas atoms with heavy W target atoms, the energy of the atoms after being reflected from the target surface is dependent on its initial energy, the masses of the atoms involved in the collision and the incident angle of the impinging atom. Considering the kinetic formula of elastic collision in case for backscattering at 180°,[38] He still carries more than 90% of its initial energy after being backscattered at the W target. Since Ar has an atomic mass nearly ten times greater than that of He, the energy of the Ar atom after an elastic collision is a factor of about 2.2 lower, leaving it with only 41% of its initial energy. Taking in to account that further energy is lost by collisions with other gas atoms in the plasma region, He has a higher probability than Ar traversing the mentioned plasma region and reaching the sample.[34,35,38] The cathode voltage of the magnetron which determines the energy range of the impinging gas atom on the target varies with the helium percentage as it can be seen in Figure 2. In the case when an excess of He is used, the energy of the backscattered He gas atom is approximately 300 eV. Taking into account the mean free path of He at 2 Pa was 12 cm, a distance target substrate of 5 cm and an energy loss in collisions in the glow-discharge region, the energy of the projectile can be assumed to further decrease to approximately its half when arriving on the sample.[35] Thus, He is estimated to have an energy of about 150 eV when impinging the sample.

The strong change in film structure observed when He (92%) is used in the process gas mixture is assigned to the dynamic incorporation of He into the growing film. Arguing from film growth mechanisms, He may hinder the coarsening of formed islands and forces incoming tungsten atoms to undergo renucleation on the existing film structure.[36] Because interstitial diffusion of He in W is already high at RT,[28] clusters and bubbles will probably form during the coating process inducing distortions of the film giving it a high degree of porosity. As a result the total number of grain boundaries increases massively, providing a larger inventory space for He. At elevated surface temperatures, desorption of newly adsorbed He increases whereas the number of lattice defects probably decreases, which was shown to result in a lower concentration of He inside a deposited film.[34] Moreover, the thermal energy enables the already incorporated He to diffuse; leading on one hand to He losses because of desorption, but on the other hand, promotion of He bubble coalescence able to distort the W lattice and induce nanostructuring. In other words, the effect on He uptake of depositing at high temperatures can be 2-fold. Although it probably leads to a reduced efficiency in He incorporation into the film,[34] it may induce stronger structural modifications due to not only the diffusion of He clusters but also to W atoms themselves.

The loading of the W coating with He was confirmed by GDOES measurements. It has been previously shown that good results regarding the amount of entrapped He in W could be achieved with this method.[39] Figure 4 shows the outcome for

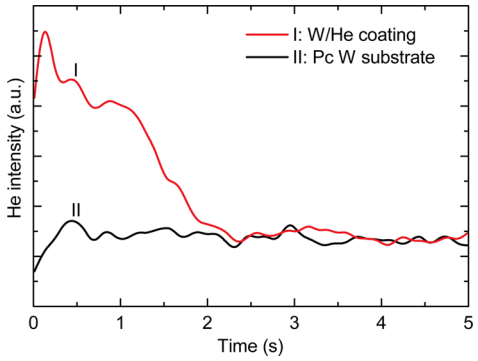

Figure 4. GDOES measurement of the He spectral line (587.5 nm) for (I) a He-loaded coating and (II) a virgin Pc W substrate as reference. Note that for (I), the He-signal was measured for the entire extent of the film. Ne was used as the working gas at an erosion rate of 6.5 μm/min.

(I) the W coating prepared with 92% He (Figure 2c) and (II) a virgin Pc W substrate as a reference. The plot shows the measured intensity of He's spectral line (587.5 nm) with respect to the time. Considering an erosion rate of about 6.5 μm/min, the duration is directly proportional to the depth of the specimen. The examined thin film was only few hundreds of nm thick. Therefore, the He signal of the He-loaded film (I) dropped to the background level in less than 3s. However, the results confirm efficient incorporation of He inside the film as the signal is initially considerably high at first and then drops rapidly to reference level when the substrate is reached. A conclusion about the distribution of the He concentration throughout the film is difficult to draw from the measurement; however, it was shown that He is uniformly embedded during deposition of titanium using a He/Ar mixture comparable to ours, 95% He for ref 34 and 93% He for ref 35.

Effects of Thermal Unloading on the Helium-Loaded Coatings. The influence of the surface temperature was investigated by various experiments such as thermal desorption measurements, an annealing experiment and plasma treatments at various surface temperatures. The coating using a gas mixture of 92% He at 1000 K (Figure 2c) was prepared and transferred to the high-T facility where thermal desorption was carried out, i.e., the sample was exposed to air in between. The desorption profile of helium is important during helium loading, as it is an equilibrium process of implantation and desorption. Kajita et al.[23] have recently reported the likelihood of a flux threshold for inducing fuzz nanostructures by He irradiation. Although the He ion flux determines the number of He implanted, the temperature and the population of the different He binding types determines the desorption rate.

Figure 5 shows the results of the thermal desorption measurements. The experiment was performed twice using different temperature sweep rates of ~93 and ~25 K/min. The He leak rate is displayed as a function of time. The simultaneously measured temperature is shown on the right y-axis in red. A measurement of the background is added to the lower diagram (blue curve), which confirms a flat, negligible background. Distinct desorption peaks were measured at ca.

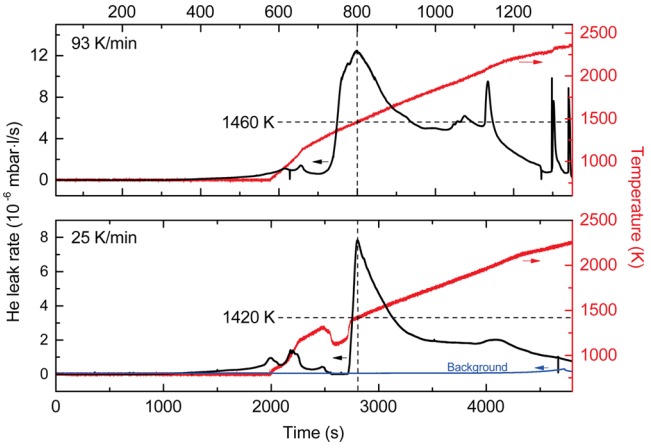

Figure 5. Thermal desorption measurements for a W coating prepared with 92% He. The He leak rate is plotted versus time. The temperature was measured simultaneously with a pyrometer (red curve and right *y*-axis). The top diagram shows a fast temperature sweep (~93 K/min) and the bottom one shows a slow one (~25 K/min). The blue curve shows measurement of the background as a virgin substrate was heated.

820, 1000, 1420, and 2000 K. The temperatures were taken from the slower sweep because it is probably more accurate since the retardation of the detection of desorbed He is lower. The existence of distinct peaks are consistent with the suggestion of different binding strengths of He to vacancies throughout the film. The temperature indicates the activation energy needed to overcome these binding energies. Depending on the number of helium atoms at a trap site, the binding energy of single helium atoms varies greatly. The thermal desorption study by Baldwin et al.[19] indicates the desorption peak positions of a He atom depending on how many He are occupying a vacancy (He_n-V) based on findings of Kornelsen et al.[40] According to this, the binding energy of He in a singly occupied vacancy is 4.0 eV corresponding to a temperature of 1560 K. The binding energy to a vacancy weakens as the number of He in the same vacancy increases from 1 to 10. For instance, He desorbs from He_2−V at 1220 K. However, at around 10 He atoms, the cluster of He is able to displace adjacent W atoms and gets effectively immobilized.[30] As a consequence of this, the desorption peaks are shifted to higher temperatures as the cluster grows. In our measured desorption profile, the maximum desorption was found to be at about 1420 K and is assigned to the desorption peak for a single He occupying a vacancy[28] even though it differs by 0.36 eV, which is believed to be in the error range of the temperature measurement. The peak found at around 1000 K is assigned to doubly (or even multiply) occupied vacancies, whereas the broad peak at 2000 K can be related to formation of clusters.[19] In the study of Baldwin et al.,[19] the He implantation was carried out by low-flux He plasma exposure ($\Gamma_{He^+} = 4.0 \times 10^{20}$ m^{-2} s^{-1}) and fuzz-like growth on the surface was observed when an incident ion energy of 57 eV was used. In their case, most of the He originated from traps where two helium atoms were bound to a single vacancy (He_2−V). In the current case, where He was entrapped during the deposition process, He from a singly occupied vacancy was released dominantly. The obtained thermal desorption measurement also offers a way to roughly estimate the relative He content in the film. By applying the ideal gas equation for the integrated profile shown in Figure 5, the total number of He can be obtained, which is 1.16×10^{17}. Assuming the deposited W film to have dimensions of 3 mm × 30 mm × 250 nm, this results in a He/W ratio of the film of roughly 0.087. This value is assumed to be higher when the coating is performed at RT because lots of He atoms desorb as a consequence of the elevated temperatures.

Figure 6 shows SEM images of W coatings with 92% He in the process gas after (a) 2 h annealing and (b−d) 2 h helium plasma exposure. The surface morphology of the coating prior to the treatments is in Figure 2c. The annealing experiment was conducted in situ, while the plasma treatments at different temperatures were performed at the high-T facility and, therefore, were exposed to air for the transfer. For the plasma exposures, the sample was biased with a DC voltage of −50 V. The resulting ion energy is therefore the difference between the positive plasma potential V_p and the DC bias set on the sample, V_{bias}. The plasma potential was measured with a Langmuir probe in another facility with an identical plasma source and, is therefore, believed to be around 45−50 V, which results in an

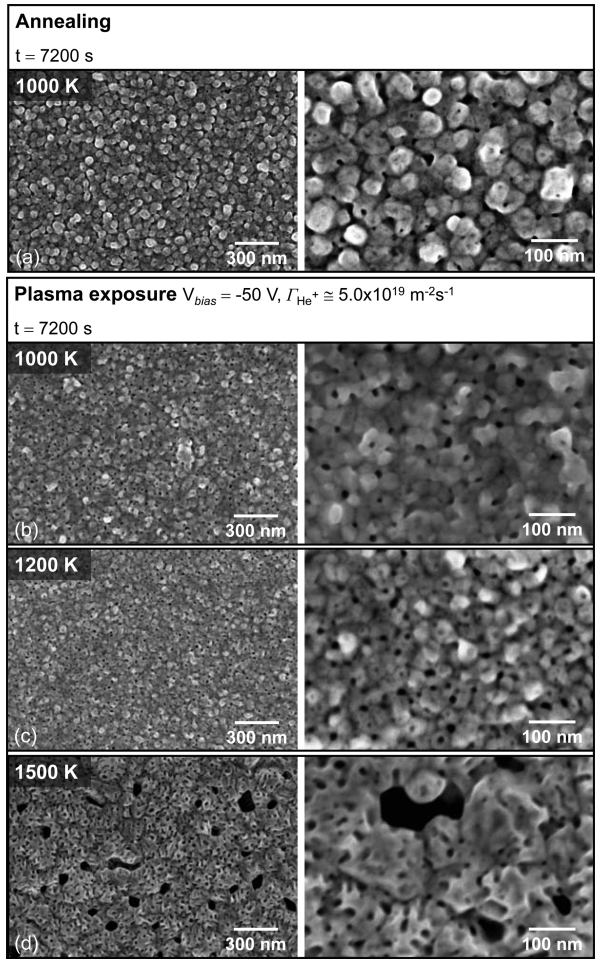

Figure 6. Top view SEM images of the W coating prepared using 92% He after various experiments. (a) Annealing of the coating results in the moderate formation of pinholes while the overall surface morphology is maintained. (b) Plasma exposure applying a DC bias of −50 Vat 1000 K results in enhanced development of pinholes. (c) At 1200 K, a higher density of pinholes is observed as the initial granular surface remains. (d) At 1500 K, strong structuring of the surface is achieved exhibiting pinholes together with very large voids. The transformation can be linked to massive unloading of the film as suggested in Figure 5

ion energy of approximately 100 eV. According to SRIM calculations and Yamamura et al.,[32] this is still below the damage threshold for He on W which lies around 150 eV. After annealing at 1000 K (Figure 6a), the low magnification image revealed only little effect on the surface since a granular structure as in Figure 2c is observed. Although the granular grains were maintained, the number of pinholes increased. At a higher magnification though, a lot of holes ranging from little pinholes to larger voids became visible. This observation is attributed to desorption of pre-embedded He in the film. The thermal desorption profile of the coating exhibits desorption peaks already at around 800 K (see Figure 5). It can therefore be concluded that the elevated temperature activates trapped He and He clusters in an Arrhenius-type reaction, which then coalesce with others to form highly pressurized bubbles. At this point, the process is similar to mechanism of fuzz formation suggested by Kajita et al.[22] or described earlier in section. When the surface temperature was set approximately to 1000 K during the plasma treatment (Figure 6b), the obtained surface is comparable to the annealing experiment in Figure 6a as pinholes can be observed and the topography is not significantly altered. The holes, which are probably a consequence of rupture because of bubble formation underneath the surface, appear between the roundly shaped grains. The outcome can be interpreted as an effect of both; He implantation from the plasma exposure and He desorption of pre-embedded He. In contrast to this experiment, the effect of the two processes alone are shown in previous images: The outcomes in Figure 1 are solely a consequence of He implantation as no He-filled coating was prepared for this experiment. The effect of only the He desorption at 1000 K is depicted in Figure 6a as a He-loaded coating was annealed. It should be noted that the results shown in Figure 1 were achieved by applying RF to the sample, whereas a DC voltage was applied during the plasma exposures in the high-T facility (Figure 6b–d). Pinholes result from both of the processes which is attributed to growth of He bubbles beneath the surface. A similar, but enhanced outcome is obtained when the sample is heated up to 1200 K (Figure 6b). The density of pinholes increased, whereas the granular structure can still be distinguished. However, when the surface temperature was set to 1500 K (Figure 6c), strong topographic changes could be observed. The obtained structure consists of larger voids in the order of 100 nm together with the previously observed pinholes. Considering the thermal desorption profile in Figure 5, it can be seen that the highest intensity peak is close to 1500 K; hence, the strong surface modification is assumed to be an effect of massive unloading of He atoms. At this temperature, activation of most of the He occurs which accelerates and enhances the nucleation and growth of bubbles. Additionally, 1500 K is probably already in the range of the recrystallization temperature which starts between 1500 and 1700 K, depending on the grade and fabrication method.[21] At 1000 and 1200 K, only a small fraction of the entrapped He is activated since only small desorption signals were measured below 1200 K. This leads to a modest change of the structure. He implantation by the plasma exposure which also gives rise to pinholes (as discussed in section) is in addition to the effect of desorption as these two processes can be assumed to be in equilibrium. As the plasma source was operated at 150 W and a −50 V DC bias was applied on to the sample in order to maintain the conditions of the plasma exposures, desorption of He dominates at 1500 K, resulting in a significant change of the surface topography.

CONCLUSION

In summary, exposure of polycrystalline and nanocrystalline tungsten samples to a low-flux ($\sim 1 \times 10^{19}$ m^{-2} s^{-1}) helium plasma accessible in a common laboratory setup showed promising signs of surface structuring comparable to an early stage of fuzz-like growth. Even though, a certain flux is believed to be surmounted to receive the final tendril structure, considerable surface roughening and porosity could be induced. Tungsten coatings in a predominant He atmosphere were performed in order to investigate He loading during deposition and its effect of He on thin film microstructure. The use of 92% He and 8% Ar induced high level of porosity to the deposited films, which is attributed to He changing the typical film growth process by hindering coarsening and forcing renucleation. The incorporation of He during the coating process is clearly confirmed with a qualitative GDOES measurement. Thermal desorption measurements on the same type of coating (prepared at 1000 K) further allowed a study of population of various traps (He_n-V). Massive unloading of He was observed at around 1500 K, which is assigned to single He bound to a single vacancy. Other prominent peaks were attributed to He originating from doubly occupied vacancies (~1000 K) and larger clusters (~2000 K). Plasma exposure at different temperatures showed an enhanced formation of pinholes with increasing temperatures resulting in a complete surface transformation at 1500 K, which can be linked to the previously mentioned strong desorption of He. From the work presented here, it can be concluded that the activation of the preimplanted He and its unloading induces strong morphological changes. Thus, formation of nanostructures by He plasma irradiation without the use of high-flux plasma devices can be obtained by loading the material with He prior to the exposure. If the amount of He bubbles suffices, nanostructured materials applicable in a variety of fields can be obtained with common (low-flux) laboratory plasma sources.

AUTHOR INFORMATION

Corresponding Author

*E-mail: laurent.marot@unibas.ch.

Notes

The authors declare no competing financial interest.

ACKNOWLEDGMENTS

The authors thank the Swiss Federal Office of Energy and the Federal Office for Education and Science for their financial support. This work was also supported by the Swiss National Foundation (SNF) and the National Center of Competence in Research on Nanoscale Science (NCCR-Nano).

REFERENCES

(1) Gleiter, H. Nanostructured Materials: Basic Concepts and Microstructure. *Acta Mater.* **2000**, *48*, 1–29.

(2) Nalwa, H. S. *Nanostructured Materials and Nanotechnology: Concise Edition*; Academic Press: San Diego, CA, 2001.

(3) Seal, S. *Functional Nanostructures: Processing, Characterization, and Applications*; Nanostructure Science and Technology; Springer: New York, NY, 2008.

(4) Aricò, A. S.; Bruce, P.; Scrosati, B.; Tarascon, J.-M.; Van Schalkwijk, W. Nanostructured Materials for Advanced Energy Conversion and Storage Devices. *Nat. Mater.* **2005**, *4*, 366–377.

(5) van de Krol, R.; Liang, Y.; Schoonman, J. Solar Hydrogen Production with Nanostructured Metal Oxides. *J. Mater. Chem.* **2008**, *18*, 2311–2320.

(6) Su, J.; Guo, L.; Bao, N.; Grimes, C. A. Nanostructured WO_3/$BiVO_4$ Heterojunction Films for Efficient Photoelectrochemical Water Splitting. *Nano Lett.* **2011**, *11*, 1928−1933.
(7) de Respinis, M.; De Temmerman, G.; Tanyeli, I.; van de Sanden, M. C.; Doerner, R.; Baldwin, M.; van de Krol, R. Efficient Plasma Route to Nanostructure Materials: Case Study on the Use of m-WO_3 for Solar Water Splitting. *ACS Appl. Mater. Interfaces* **2013**, *5*, 7621−7625.
(8) Kajita, S.; Yoshida, T.; Kitaoka, D.; Etoh, R.; Yajima, M.; Ohno, N.; Yoshida, H.; Yoshida, N.; Terao, Y. Helium Plasma Implantation on Metals: Nanostructure Formation and Visible-Light Photocatalytic Response. *J. Appl. Phys.* **2013**, *113*, 134301.
(9) Kajita, S.; Yokochi, T.; Ohno, N.; Kumano, T. Near Infrared Radiation from Heated Nanostructured Tungsten. *Jpn. J. Appl. Phys.* **2012**, *51*, 01AJ03.
(10) Rephaeli, E.; Fan, S. Tungsten Black Absorber for Solar Light with Wide Angular Operation Range. *Appl. Phys. Lett.* **2008**, *92*, 211107−211107.
(11) Ohno, N.; Hirahata, Y.; Yamagiwa, M.; Kajita, S.; Takagi, M.; Yoshida, N.; Yoshihara, R.; Tokunaga, T.; Tokitani, M. Influence of Crystal Orientation on Damages of Tungsten Exposed to Helium Plasma. *J. Nucl. Mater.* **2013**, *438*, S879−S882.
(12) Takamura, S.; Ohno, S.; Nishijima, D.; Kajita, S. Formation of Nanostructured Tungsten with Arborescent Shape due to Helium Plasma Irradiation. *Plasma Fusion Res.* **2006**, *1*, 051−051.
(13) Tanyeli, I.; Marot, L.; van de Sanden, M. C.; De Temmerman, G. Nanostructuring of Iron Surfaces by Low-Energy Helium Ions. *ACS Appl. Mater. Interfaces* **2014**, *6*, 3462−3468.
(14) Sakamoto, R.; Muroga, T.; Yoshida, N. Microstructural Evolution Induced by Low Energy Hydrogen Ion Irradiation in Tungsten. *J. Nucl. Mater.* **1995**, *220*−*222*, 819−822.
(15) Nakamura, Y.; Kitajima, S.; Shinohara, K. Influence of 100 keV Helium Irradiation on Tensile Properties of Pure Iron and JFMS Steel at Low Temperatures. *J. Nucl. Mater.* **1989**, *169*, 185−197.
(16) Baldwin, M.; Doerner, R. Helium Induced Nanoscopic Morphology on Tungsten under Fusion Relevant Plasma Conditions. *Nucl. Fusion* **2008**, *48*, 035001.
(17) Baldwin, M.; Doerner, R.; Nishijima, D.; Tokunaga, K.; Ueda, Y. The Effects of High Fluence Mixed-Species (Deuterium, Helium, Beryllium) Plasma Interactions with Tungsten. *J. Nucl. Mater.* **2009**, *390*, 886−890.
(18) Baldwin, M.; Doerner, R. Formation of Helium Induced Nanostructure Fuzz on various Tungsten Grades. *J. Nucl. Mater.* **2010**, *404*, 165−173.
(19) Baldwin, M.; Lynch, T.; Doerner, R.; Yu, J. Nanostructure Formation on Tungsten Exposed to Low-Pressure RF Helium Plasmas: A Study of Ion Energy Threshold and Early Stage Growth. *J. Nucl. Mater.* **2011**, *415*, S104−S107.
(20) Sakaguchi, W.; Kajita, S.; Ohno, N.; Takagi, M.; Kurishita, H. Formation Condition of Fiberform Nanostructured Tungsten by Helium Plasma Exposure. *Plasma Fusion Res.* **2010**, *5*, S1023−S1023.
(21) De Temmerman, G.; Bystrov, K.; Zielinski, J. J.; Balden, M.; Matern, G.; Arnas, C.; Marot, L. Nanostructuring of Molybdenum and Tungsten Surfaces by Low-Energy Helium Ions. *J. Vac. Sci. Technol., A* **2012**, *30*, 041306−041306.
(22) Kajita, S.; Sakaguchi, W.; Ohno, N.; Yoshida, N.; Saeki, T. Formation Process of Tungsten Nanostructure by the Exposure to Helium Plasma under Fusion Relevant Plasma Conditions. *Nucl. Fusion* **2009**, *49*, 095005.
(23) Kajita, S.; Ohno, N.; Yajima, M.; Kato, J. Growth Annealing Equilibrium of Tungsten Nanostructures by Helium Plasma Irradiation in Non Eroding Regimes. *J. Nucl. Mater.* **2013**, *440*, 55−62.
(24) Wisse, M.; Eren, B.; Marot, L.; Steiner, R.; Meyer, E. Spectroscopic Reflectometry of Mirror Surfaces During Plasma Exposure. *Rev. Sci. Instrum.* **2012**, *83*, 013509−013509.
(25) Eren, B.; Marot, L.; Langer, M.; Steiner, R.; Wisse, M.; Mathys, D.; Meyer, E. The Effect of Low Temperature Deuterium Plasma on Molybdenum Reflectivity. *Nucl. Fusion* **2011**, *51*, 103025.
(26) Siegel, R.; Howell, J. R. *Thermal Radiation Heat Transfer*, 4th ed; Taylor and Francis: New York, 2002.
(27) Ziegler, J. F. *SRIM−The Stopping and Range of Ions in Matter*, version SRIM-2008; collection of software packages which calculate many features of the transport of ions in matter; www.srim.org.
(28) Kornelsen, E. The Interaction of Injected Helium with Lattice Defects in a Tungsten Crystal. *Radiat. Eff.* **1972**, *13*, 227−236.
(29) Nishijima, D.; Ye, M.; Ohno, N.; Takamura, S. Incident Ion Energy Dependence of Bubble Formation on Tungsten Surface with Low Energy and High Flux Helium Plasma Irradiation. *J. Nucl. Mater.* **2003**, *313*, 97−101.
(30) Sefta, F.; Hammond, K. D.; Juslin, N.; Wirth, B. D. Tungsten Surface Evolution by Helium Bubble Nucleation, Growth and Rupture. *Nucl. Fusion* **2013**, *53*, 073015.
(31) Kajita, S.; Yoshida, N.; Yoshihara, R.; Ohno, N.; Yamagiwa, M. TEM Observation of the Growth Process of Helium Nanobubbles on Tungsten: Nanostructure Formation Mechanism. *J. Nucl. Mater.* **2011**, *418*, 152−158.
(32) Yamamura, Y.; Tawara, H. Energy Dependence of Ion-Induced Sputtering Yields from Monatomic Solids at Normal Incidence. *At. Data Nucl. Data Tables* **1996**, *62*, 149−253.
(33) Powder Diffraction File, Card no. 04−0806, Joint Committee on Powder Diffraction Standards, 1953.
(34) Hong-Chao, P.; Shun-Zhong, L.; Xing-Gui, L.; Zhu, A.; Ning, L.; Yan-Min, D.; Xing-Chun, W.; Ben-Fu, Y.; Pei-Lu, W.; Si-Xiao, Z. Effects of Substrate Temperature on Helium Content and Microstructure of Nanocrystalline Titanium Films. *Chin. Phys. Lett.* **2006**, *23*, 3238.
(35) Liu, C.-Z.; Shi, L. Q.; Zhou, Z. Y.; Hao, X. P.; Wang, B. Y.; Liu, S.; Wang, L. B. Investigations of Helium Incorporated into a Film Deposited by Magnetron Sputtering. *J. Phys. D: Appl. Phys.* **2007**, *40*, 2150.
(36) Thompson, C. Structure Evolution during Processing of Polycrystalline Films. *Annu. Rev. Mater. Sci.* **2000**, *30*, 159−190.
(37) Barna, P.; Adamik, M. Fundamental Structure Forming Phenomena of Polycrystalline Films and the Structure Zone Models. *Thin Solid Films* **1998**, *317*, 27−33.
(38) Chu, W.-K. *Backscattering Spectrometry*; Academic Press: San Diego, CA, 1978.
(39) Hatano, Y.; Shi, J.; Yoshida, N.; Futagami, N.; Oya, Y.; Nakamura, H. Measurement of Deuterium and Helium by Glow-Discharge Optical Emission Spectroscopy for Plasma−Surface Interaction Studies. *Fusion Eng. Des.* **2012**, *87*, 1091−1094.
(40) Kornelsen, E.; Van Gorkum, A. A Study of Bubble Nucleation in Tungsten using Thermal Desorption Spectrometry: Clusters of 2 to 100 Helium Atoms. *J. Nucl. Mater.* **1980**, *92*, 79−88.